CrystEngComm

ROYAL SOCIETY OF CHEMISTRY

PAPER

View Article Online
View Journal | View Issue

Cite this: *CrystEngComm*, 2025, **27**, 3041

Calix[4]arene-supported trigonal and square prisms of Mn and Na†

Lucinda R. B. Wilson, [a] Scott J. Dalgarno *[b] and Euan K. Brechin *[a]

Received 14th March 2025,
Accepted 9th April 2025

DOI: 10.1039/d5ce00285k

rsc.li/crystengcomm

The heterometallic tricapped trigonal prism $[Mn^{III}_3Na_6(TBC[4])_3(CO_3)(Cl)(dmso)_7]\cdot 5MeCN$ ($[Mn_3Na_6]$; **1**·5MeCN) and the related heterometallic tetracapped square prism $[Mn^{III}_4Mn^{II}_2Na_6(bisTBC[4])_2(CO_3)_2(Cl)_2(dmf)_8(MeOH)_{1.2}(H_2O)_{0.8}]\cdot 6MeCN$ ($[Mn_6Na_6]$; **2**·6MeCN), are isolated using *p*-^{t}Bu-calix[4]arene (H_4TBC[4]) and 2,2′-bis-*p*-^{t}Bu-calix[4]arene (H_8-bisTBC[4]), respectively. In the former the Mn^{III} ions sit in the TBC[4] polyphenolic pockets, forming three Mn-TBC[4] metalloligands that cap the square faces of the prism, whose vertices contain the six Na ions. Introduction of the bis-calix[4]arene enables expansion of the main building block from three Mn-TBC[4] metalloligands in **1** to four Mn-TBC[4] metalloligands in **2**. The result is the formation of a square prism of Na/Mn^{II} ions, with four of the square faces capped with Mn^{III} ions. Dc magnetic susceptibility and magnetisation measurements reveal paramagnetism in **1** and weak antiferromagnetic exchange interactions in **2**.

Introduction

The synthetic versatility and accessibility of *p-tert*-butylcalix[*n*]arenes have seen them employed in an incredibly diverse range of chemistry.[1–8] In coordination chemistry, the tetraphenolic pocket of *p-tert*-butylcalix[4]arene (H_4TBC[4], Fig. 1) presents an attractive ligand motif for the construction of transition metal (TM) and lanthanide metal (LnM^{III}) metalloligands that can self-assemble into larger, polymetallic cages.[9] Structurally, this means the TM-TBC[4]/LnM-TBC[4] moiety acts as a capping fragment in the resulting metallic skeleton, with some or all of the phenolato O-atoms further bridging to other metal ions. When these metal ions are paramagnetic, the clusters can display fascinating magnetic behaviour including, for example, single-molecule magnetism,[10] spin frustration[11] or an enhanced magnetocaloric effect.[12] The dominant structure-directing role of the calix[4]arene also means that, in some cases, analogous structural topologies can be made with different metals and with metals in a variety of oxidation states, allowing detailed magneto-structural studies.[13]

The tetraphenolato pocket of $TBC[4]^{4-}$ is particularly well suited to bonding Jahn–Teller (JT) distorted ions such as octahedral Mn^{III} because it will preferentially coordinate metals possessing four short equatorial bonds.[14] Indeed, this ability has been exploited to isolate a number of polymetallic Mn clusters, including $[Mn^{III}Mn^{II}]$,[15] $[Mn^{III}Mn^{II}]_2$,[16] $[Mn^{III}_2Mn^{II}_2]$,[17] $[Mn^{III}_3Mn^{II}_2]$,[18] $[Mn^{III}_7Mn^{II}]$,[19] and $[Mn^{III}_8Mn^{II}_4]$.[20] In each case the Mn^{III} ions sits in the TBC[4] pocket, and the Mn^{III}-TBC[4] metalloligand further bridges to additional metal ions, often encapsulating a polymetallic metal-oxo/hydroxo cluster.

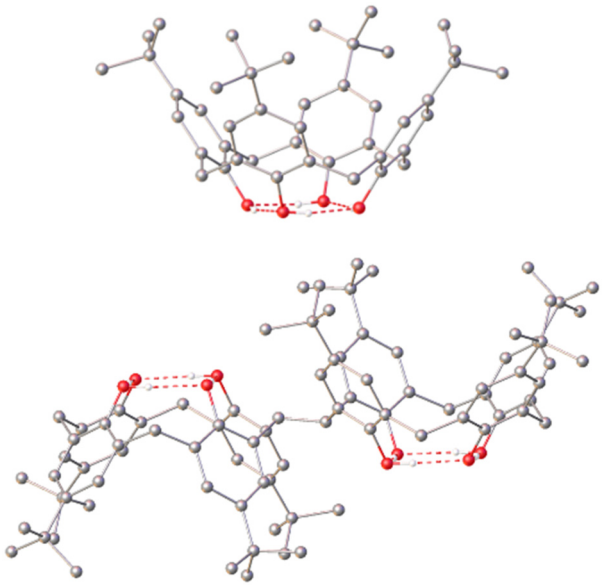

Fig. 1 The molecular structures of H_4TBC[4] (top) and H_8-bisTBC[4] (bottom). Colour code: O = red, C = grey, phenolic H atoms = white. The H atoms of the C–H bonds are omitted. The red dashed lines represent hydrogen bonding.

[a] *EastCHEM School of Chemistry, The University of Edinburgh, David Brewster Road, Edinburgh, Scotland, EH9 3FJ, UK. E-mail: ebrechin@ed.ac.uk*
[b] *Institute of Chemical Sciences, Heriot-Watt University, Riccarton, Edinburgh, Scotland, EH14 4AS, UK. E-mail: S.J.Dalgarno@hw.ac.uk*

† Electronic supplementary information (ESI) available: PXRD data, additional figures. CCDC 2430896 and 2430897. For ESI and crystallographic data in CIF or other electronic format see DOI: https://doi.org/10.1039/d5ce00285k

Extension of the chemistry to the related to 2,2′-bis-*p*-^{t}Bu-calix[4]arene[21] (H_8-bisTBC[4], Fig. 1) in which two H_4TBC[4]s are linked *via* a methylene bridge allows expansion from a single organic scaffold possessing one to two Mn^{III}-TBC[4] metalloligands. Indeed, the conformational flexibility (ring inversion) of H_8-bisTBC[4], provides an organic skeleton with eight proximal phenolic O-atoms, and this potentially offers a route to larger polymetallic cages. Indeed, in Mn chemistry this has led to the isolation of $[Mn^{III}_4Mn^{II}_6]$,[22] $[Mn^{III}_6Mn^{II}_4]$,[23] $[Mn^{III}_4Mn^{II}_4]$,[24] $[Mn^{IV}_2Mn^{III}_{10}Mn^{II}_8]$,[25] and $[Mn^{III}_{10}Mn^{II}_4]$.[26] Here we extend this family of compounds to include heterometallic species by reporting the synthesis, structure and magnetic properties of $[Mn^{III}_3Na_6(TBC[4])_3(CO_3)(Cl)(dmso)_7]$·5MeCN ($[Mn_3Na_6]$; **1**·5MeCN) and $[Mn^{III}_4Mn^{II}_2Na_6(bisTBC[4])_2(CO_3)_2(Cl)_2(dmf)_8(MeOH)_{1.2}(H_2O)_{0.8}]$·6MeCN ($[Mn_6Na_6]$; **2**·6MeCN). The former describes a tricapped trigonal prism, and the latter a tetracapped square prism. Both structure types are thus far unknown in Mn-based calix[*n*]arene chemistry.

Experimental

Synthesis

$MnCl_2·4H_2O$, NaOH, NaOPh and NEt_3 were purchased from commercial suppliers and used without further purification. *p*-^{t}Bu-calix[4]arene (H_4TBC[4]) and 2,2′-bis-*p*-^{t}Bu-calix[4]arene (H_8-bisTBC[4]) were prepared as previously described.[1,21]

$[Mn^{III}_3Na_6(TBC[4])_3(CO_3)(Cl)(dmso)_7]$·5MeCN ($[Mn_3Na_6]$; 1·5MeCN)

H_4TBC[4] (0.200 g, 0.308 mmol) and $MnCl_2·4H_2O$ (0.061 g, 0.308 mmol) were dissolved in a 1 : 1 dmso/MeOH mixture (20 mL) and stirred for 10 minutes. NaOH (0.025 g, 0.616 mmol) was added and the resulting dark purple solution stirred for 3 hours. After filtration, MeCN was diffused into the mother liquor, affording crystals of **1**·5MeCN in ∼15% yield after 5 days. Addition of Na_2CO_3 (0.065 g, 0.616 mmol) or $NaHCO_3$ (0.052 g, 0.616 mmol) increases the yield to ∼30%. Elemental analysis (%) calculated for **1** (without any solvent of crystallisation): C, 61.31%; H, 6.93%; N, 0.00%. Found: C, 61.03%; H, 6.81%, N, 0.08%.

$[Mn^{III}_4Mn^{II}_2Na_6(bisTBC[4])_2(CO_3)_2(Cl)_2(dmf)_8(MeOH)_{1.2}(H_2O)_{0.8}]$·6MeCN ($[Mn_6Na_6]$; 2·6MeCN)

H_8-bisTBC[4] (0.100 g, 0.077 mmol), $MnCl_2·4H_2O$ (0.091 g, 0.462 mmol) and NaOPh (0.054 g, 0.462 mmol) were dissolved in a 1 : 1 dmf/MeOH mixture (24 mL) and stirred for 10 minutes. NEt_3 (0.4 mL, 2.87 mmol) was added and the resulting dark purple solution stirred for 2 hours. After filtration, MeCN was diffused into the mother liquor, affording crystals of **2** in ∼8% yield after 5 days. Addition of Na_2CO_3 (0.073 g, 0.693 mmol) or $NaHCO_3$ (0.058 g, 0.693 mmol) increases the yield to ∼30%. Elemental analysis (%) calculated for **2** (without any solvent of crystallisation): C, 63.58%; H, 6.93%; N, 2.95%. Found: C, 63.21%; H, 6.84%, N, 2.57%.

Note the change from dmso to dmf in the reactions used to produce **1** and **2**, respectfully. No crystalline material was isolated when dmf was employed in the former or dmso in the latter.

X-ray diffraction

Single crystal X-ray diffraction data for **1–2** were collected on a Bruker D8 Venture diffractometer operating with CuK_α radiation (1.54178 Å) at 100(2) K. Structures were solved using ShelXT/ShelXL and refined with version 2018/3 of ShelXL interfaced through Olex2.[27–29] All non-hydrogen atoms were refined anisotropically. Hydrogen atom positions were calculated geometrically and refined using the riding model. Disorder was handled using partial occupancies and appropriate restraints. Crystal data for **1** (CCDC 2430896): $C_{318}H_{432}Cl_2Mn_6N_{12}Na_{12}O_{44}S_{14}$, M = 6251.99 g mol^{-1}, monoclinic, space group $C2/c$ (no. 15), a = 34.6511(7) Å, b = 20.6506(5) Å, c = 24.2274(6) Å, β = 100.104(2)°, V = 17067.4(7) Å^3, Z = 2, T = 100(2) K, μ(CuKα) = 3.371 mm^{-1}, D_{calc} = 1.217 g cm^{-3}, 16 571 reflections measured (5.948° ≤ 2θ ≤ 145.022°), 16 571 unique (R_{sigma} = 0.0903) which were used in all calculations. The final R_1 was 0.1094 ($I > 2\sigma(I)$) and wR_2 was 0.2844 (all data). Crystal data for **2** (CCDC 2430897): $C_{212.2}H_{274.6}Cl_2Mn_6N_{14}Na_6O_{32}$, M = 4071.92 g mol^{-1}, triclinic, space group $P\bar{1}$ (no. 2), a = 17.5535(4) Å, b = 18.1099(4) Å, c = 20.5110(5) Å, α = 91.090(2)°, β = 110.5190(10)°, γ = 109.8950(10)°, V = 5670.9(2) Å^3, Z = 1, T = 100(2) K, μ(CuKα) = 3.497 mm^{-1}, D_{calc} = 1.192 g cm^{-3}, 223 893 reflections measured (8.552° ≤ 2θ ≤ 148.976°), 23 081 unique (R_{int} = 0.0697, R_{sigma} = 0.0542) which were used in all calculations. The final R_1 was 0.1178 ($I > 2\sigma(I)$) and wR_2 was 0.4061 (all data).

Powder X-ray diffraction data for **1–2** were collected on polycrystalline powders using a Bruker D8 ADVANCE with Cu radiation at 40 kV, 40 mA and a Johansson monochromator, 2 mm divergence slit, 2.5 degree Soller slits on the incident beam side, LynxEye detector and Bruker DIFFRAC software. Diffraction data were measured from 2θ = 2.5–20°; step size, 0.0101°. Freshly prepared crystalline powders were loaded into borosilicate capillaries with a 0.7 mm inside diameter and measured while spinning (Fig. S1†).

Magnetic data

Magnetic susceptibility and magnetisation data were collected on powdered microcrystalline samples of **1–2** using a Quantum Design PPMS Dynacool. Susceptibility data were collected in the T = 2–300 K range under an applied magnetic field, B = 0.1 T. Magnetisation data were collected in the T = 3–10 K and B = 0.5–9.0 T ranges. A unit cell check was performed prior to measurement. Powdered samples were restrained in eicosane.

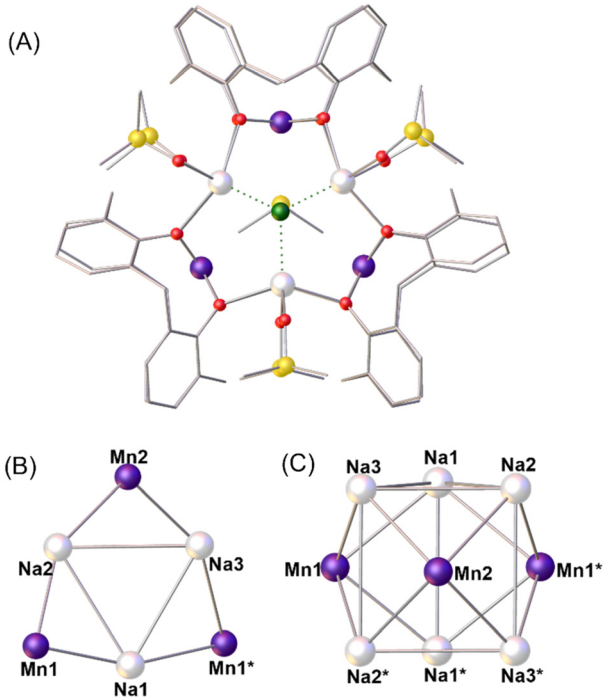

Fig. 2 A) The molecular structure of complex **1** ([Mn_3Na_6]) viewed down the *c*-axis of the cell. B) and C) Orthogonal views of the metallic skeleton/tricapped trigonal prism, with the Na ions sitting on the six vertices of the trigonal prism and the three Mn ions capping the square faces. Colour code: Mn^{III} = dark purple, Na = white, O = red, C = grey, S = yellow, Cl = green. H atoms, ^{t}Bu groups of TBC[4], the disordered carbonate ion and solvent molecules are omitted for clarity. Additional figures are provided in the ESI.† * = symmetry equivalent.

Results and discussion

Reaction of $MnCl_2{\cdot}4H_2O$ with H_4TBC[4] in a basic dmso/MeOH mixture affords single crystals of formula [$Mn^{III}{}_3$-Na_6(TBC[4])$_3$(CO_3)(Cl)(dmso)$_7$]·5MeCN ([Mn_3Na_6]; **1**·5MeCN, Fig. 2 and S2†) following diffusion of MeCN into the mother liquor. The crystals were found to be in a monoclinic cell and structure solution was carried out in the space group *C*2/*c* with the asymmetric unit (ASU) comprising half of the formula.

The metallic skeleton describes a [$Mn^{III}{}_3Na_6$] tricapped trigonal prism with the Na ions sitting on the vertices and the Mn ions capping the square faces. A disordered μ_9-$[CO_3]^{2-}$ ion sits in the centre of the cage, bonding to all nine metal ions (Mn–O, ~2.14–2.21 Å; Na-O, ~2.43–2.48 Å). The square pyramidal Mn ions sit in the phenolic TBC[4] pockets and thus have [MnO_5] coordination geometries with a sixth, longer contact to a MeCN molecule of crystallisation that sits in the TBC[4] cavity (~4.1 Å). The Mn–O(carbonate) bond (~2.14–2.21 Å) is significantly longer than the four Mn–O (phenoxide) bonds (~1.92–1.93 Å). The TBC[4] ions are all in their maximal μ_5-bridging mode, each O-arm bonded to a Mn ion and further bridging to a Na ion, thus directing the formation of square pyramidal [$MnNa_4$(TBC[4])] building blocks (for example as shown by Mn2, Na2, Na3, Na2* and Na3* in Fig. 2C, * = symmetry equivalent). The triangular [Na_3] faces of the prism are capped by a disordered mixture of one μ_3-Cl^- ion (Na···Cl, ~2.6–2.7 Å) and one dmso molecule (Na···O, ~2.4–2.6 Å), both present at 50% occupancy. The latter is asymmetrically situated with one Na–O distance of ~2.58 Å and two Na–O distances in the range ~2.42–2.48 Å. The remaining site on each 5-coordinate, distorted square pyramidal Na ion is occupied by a dmso molecule. The Na ions in **1** originate from the NaOH employed to deprotonate the H_4TBC[4] ligands, and the $[CO_3]^{2-}$ ion from the fixation of atmospheric CO_2. Deliberate addition of carbonate in the form of Na_2CO_3 or $NaHCO_3$ increases the yield of **1** approximately two-fold (see the experimental section for details). We note the structure of **1** is rather similar to the TBC[4]-supported tricapped trigonal prisms [$Cu^{II}{}_9(OH)_3$(TBC[4])$_3Cl_2$(dmso)$_{5.5}$(EtOH)$_{0.5}$][$Cu^{I}Cl_2$] and [$Cu^{II}{}_9(OH)_3$(TBC[4])$_3$(NO_3)$_2$(dmso)$_6$](NO_3).[30] However, the Cu^{II}-based cages do not contain a $[CO_3]^{2-}$ ion and neighbouring vertex Cu^{II} ions in the trigonal prism are connected to each other with μ-OH^- ions. Alongside the larger anionic radius of Na, the result is that the dimensions of the prisms are rather different, with [Mn_3Na_6] being "taller and thinner" than the "shorter and wider" [Cu_9] (Fig. S3†). Comparison of these [Cu_9] and [Mn_3Na_6] cluster motifs shows remarkable similarity despite the marked change in the anions present in the centre of the cores, 3 × μ-OH^- or 1 × μ_9-$CO_3{}^{2-}$ respectively. This warrants further investigation into the nature of the anions in this general tricapped trigonal prismatic cluster topology, results of which will be reported in due course.

Examination of the extended structure found in **1** reveals similar packing behaviour to that observed for [Cu_9] analogues.[16,31] As in those examples, the overall triangular shape of **1** drives packing of symmetry equivalents to form layers in the *ab* plane (Fig. S4†) in which TBC[4] cavities are arranged opposite regions in clusters that are reminiscent of H_4TBC[4] itself.[31] Although it is impossible for such species to form bi-layers that are preferred by solvates of TBC[4], these assemblies do display bi-layer type behaviour within layers. Inspection of the extended structure reveals the closest inter-cluster $Mn^{III}\cdots Mn^{III}$ distance to be ~15.7 Å, and between layers this is shorter at ~12.7 Å. In both cases these are well-isolated by the TBC[4] ligands and packing of the assemblies.

Extension of this chemistry to the related to 2,2′-bis-*p*-^{t}Bu-calix[4]arene (H_8-bisTBC[4], Fig. 1) affords a tetracapped square prism. Reaction of $MnCl_2{\cdot}4H_2O$ with H_8-bisTBC[4] and NaOPh in a basic dmf/MeOH mixture affords single crystals of formula [$Mn^{III}{}_4Mn^{II}{}_2$-Na_6(BisTBC[4])$_2$(CO_3)$_2$(Cl)$_2$(dmf)$_8$(MeOH)$_{1.2}$(H_2O)$_{0.8}$]·6MeCN ([Mn_6Na_6]; **2**·6MeCN) following diffusion of MeCN into the mother liquor (Fig. 3 and S5†). The crystals were found to be in a triclinic cell and structure solution was carried out in the space group $P\bar{1}$ with the ASU comprising half of the formula. The metallic skeleton describes a [$Mn^{III}{}_4Mn^{II}{}_2Na_6$] tetracapped square prism with the Mn^{II}/Na ions sitting on

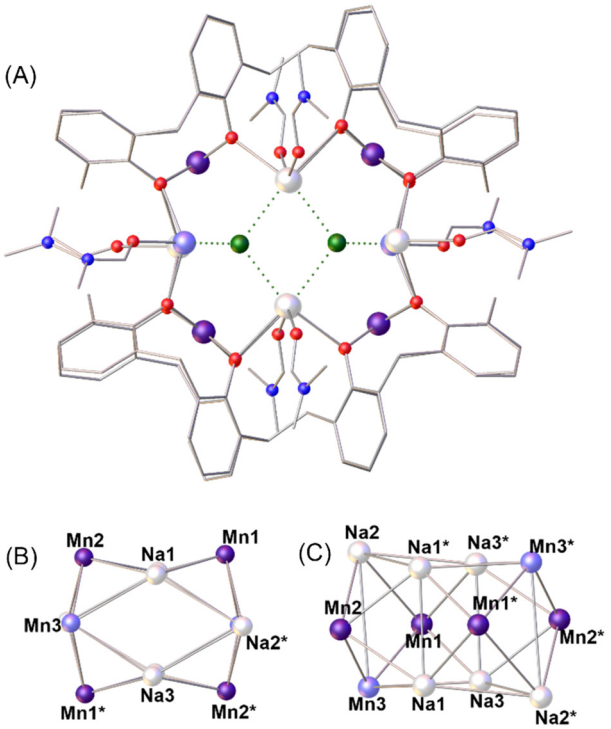

Fig. 3 A) The molecular structure of complex **2** ($[Mn_6Na_6]$) viewed down the *c*-axis of the cell. B) and C) Orthogonal views of the metallic skeleton of **2**. Colour code: Mn^{III} = dark purple, Mn^{II} = light purple, Na = white, O = red, C = grey, N = blue, Cl = green. H atoms, ᵗBu groups of H_8-bisTBC[4], carbonate ions and solvent molecules are omitted for clarity. Additional figures are included in the ESI.† * = symmetry equivalent.

the vertices of the square prism and the Mn^{III} ions capping the square faces. Disordered μ_6-$[CO_3]^{2-}$ ions occupy the inside of the cage, bridging between four vertex metal ions (Na1–3, Mn3) and two capping metal ions (Mn1*, Mn2). The four face-capping Mn^{III} ions are housed in the polyphenolic pockets of the two fully deprotonated bis-calixarene ligands whose O-atoms further bridge to the Mn^{II}/Na^{I} ions in the square prism. The fully deprotonated bisTBC[4]$^{8-}$ ligands adopt their maximal μ_8-bridging mode and thus wrap around the four square faces of the prism, completely encapsulating the $[Mn^{III}_4Mn^{II}_2Na_6(CO_3)_2]$ moiety.

The 'upper' and 'lower' square faces of the prism (as drawn in Fig. 3A and S5†) are each asymmetrically capped by a μ_3-Cl^- ion (Mn···Cl, ~2.38 Å, Na···Cl, ~2.94–3.04 Å). The Mn^{III} ions in the calix[4]arene pockets have square pyramidal $[MnO_5]$ coordination spheres, with the bonds to the four phenolic O-atoms (~1.90–2.00 Å) significantly shorter than that to the carbonate O-atom (~2.07–2.30 Å), with a sixth, longer contact to a MeCN molecule of crystallisation that sits in the TBC[4] cavity (~4 Å). The coordination spheres of the distorted square pyramidal Mn^{II} ions ($[MnO_5]$) and distorted pentagonal bipyramidal Na ions are completed by solvent molecules (MeOH, H_2O) of partial occupancy.

The packing found in the extended structure of **2** is markedly different to that outlined above for **1**. In this case the clusters are arranged diagonally side-on in the *ab* plane and form a bi-layer type arrangement as shown in Fig. S6.† The TBC[4] sub-units in the bisTBC[4]s shrouding the cluster cores are arranged such that cavities are arranged approximately opposite those of symmetry equivalent assemblies in adjacent bi-layers, behaviour that is also reminiscent of a range of H_4TBC[4] solvates.[16,31] Inspection of the structure reveals that the closest inter-cluster $Mn^{III}\cdots Mn^{III}$ distance to be ~13.1 Å, again confirming that this approach of shrouding the clusters with bulky ligands has been successful in isolating cluster cores from one another.

As for **1**, deliberate addition of carbonate in the form of Na_2CO_3 or $NaHCO_3$ increases the yield of **2**, in this case approximately four-fold (see experimental section for details). Inspection of related chemistry with Cu^{II} shows a similar structural expansion relationship upon moving from H_4TBC[4] to H_8-bisTBC[4]. The structure of **2** is reminiscent of the biscalix[4]arene-supported cluster $[Cu^{II}_{13}(bisTBC[4])_2(NO_3)(\mu\text{-}OH)_8(dmf)_7][OH]$,[24] whose metallic skeleton also describes a (centred) tetra-capped square prism (Fig. S7†). Interestingly the latter contains an encapsulated and disordered Cu^{II} ion at its centre. Like the $[Cu_9]$ cages, neighbouring vertices in the square prism in $[Cu_{13}]$ are linked to each other through μ-OH^- bridges, making $[Mn_6Na_6]$ (**2**) "taller and thinner" than the "shorter and wider" $[Cu_{13}]$. Attempts to make the 'exact' $[Mn^{II}_9]/[Mn^{II}_{13}]$ analogues of $[Cu^{II}_9]/[Cu^{II}_{13}]$ in our laboratory have failed thus far, presumably (or at least in part) due to the very strong preference for the metal ion to be Mn^{III} when housed in the TBC[4] (or C[4]) polyphenolic pocket. Indeed, there are no examples of Mn-based TBC[4] structures in the CCDC where Mn^{II} ions are coordinated in the TBC[4] pocket, and all reactions between H_4TBC[4] and Mn^{II} salts in basic solutions under standard conditions reported thus far lead to the isolation of $[Mn^{III}_2Mn^{II}_2(OH)_2(TBC[4])_2(solvent)_6]$ or analogues thereof.[17] The structure of the latter describes a $[Mn^{III}_2Mn^{II}_2]$ butterfly (or near planar diamond) in which the two 'body' Mn^{II} ions are encapsulated by two 'wing' Mn^{III}-TBC[4] metalloligands. The addition of Group I metal ions to the reaction (here Na), and the *in situ* generation of carbonate, clearly alters the reaction pathway, leading to the isolation of $[Mn_3Na_6]$ and $[Mn_6Na_6]$ multiply capped trigonal and square prisms. The average metal oxidation state in **1** and **2** is 1.67 and 2.00, respectively, perhaps suggesting that these prisms are the preferred topology for TBC[4]-supported clusters of metal ions in lower oxidation states (≤2). Interestingly, there are zero TBC[4]-supported homometallic clusters of Fe^{II}, Co^{II} or Zn^{II} reported in the literature, so it will be intriguing to discover the coordination chemistry of these metal ions. Likewise, it will be interesting to see if the incorporation of other Group I metal ions (Li, K, Cs) leads to the same structure types, and how this might change through the use of Group II metal ions (Mg–Ba). Similarly, the TBC[4]-based coordination chemistry of other combinations of M^{III}–M^{I} ions remains to be explored, as does the deliberate and

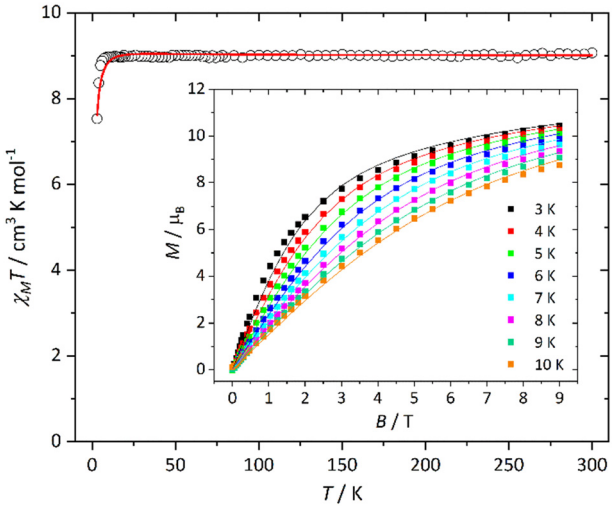

Fig. 4 Magnetic susceptibility and magnetisation (inset) data for **1**. The solid lines are a simultaneous fit of the data to spin-Hamiltonian (1). See text for full details.

systematic employment of the carbonate ion as a bridging ligand.

Magnetic measurements

Direct current magnetic susceptibility (χ) and magnetisation (M) studies were performed on polycrystalline samples of **1**–**2** in the temperature and field ranges T = 2–300 K, B = 0.1 T and T = 3–10 K, B = 0.5–9.0 T, respectively (Fig. 4 and 5). At 300 K, the χT value of ~9.0 cm^3 K mol^{-1} for **1** matches the Curie constant expected for three uncorrelated Mn^{III} ions with g = 2.0. Upon cooling, the χT product is invariant with temperature until approximately T = 8 K where it rapidly decreases to a minimum value of ~5.7 cm^3 mol^{-1} K at T = 2 K. The high temperature data are therefore suggestive of paramagnetism, with the low temperature decline assigned to a combination of zero-field splitting effects and/or very weak intra- and inter-molecular antiferromagnetic exchange interactions. Note that at these temperatures all three are likely to be correlated. The magnetisation data rise rapidly with increasing field, reaching a value of M = ~10.4 μ_B at T = 3 K and B = 9.0 T. The zero, or very weak exchange, is not surprising given that the three Mn ions are only connected to each other *via* the single, disordered $[CO_3]^{2-}$ ion lying in the centre of the cage (Fig. S2;† Mn···Mn ~5.31–5.43 Å). A simultaneous fit of the susceptibility and magnetisation data using spin-Hamiltonian (1) (without the exchange term) afforded the best fit parameters $|D_{Mn(III)}|$ = 3.7 cm^{-1} and zJ = 0.01 cm^{-1}. The value of D is line with that expected for a Jahn–Teller distorted Mn^{III} ion with a $[MnO_5]$ coordination sphere.[32]

$$\hat{H} = \sum_i D_i\left(\hat{S}_z^2 - S(S+1)/3\right) + \mu_B B \sum_i g_i \hat{S}_i - 2\sum_{i<j} J_{i,j}\hat{S}_i \cdot \hat{S}_j \quad (1)$$

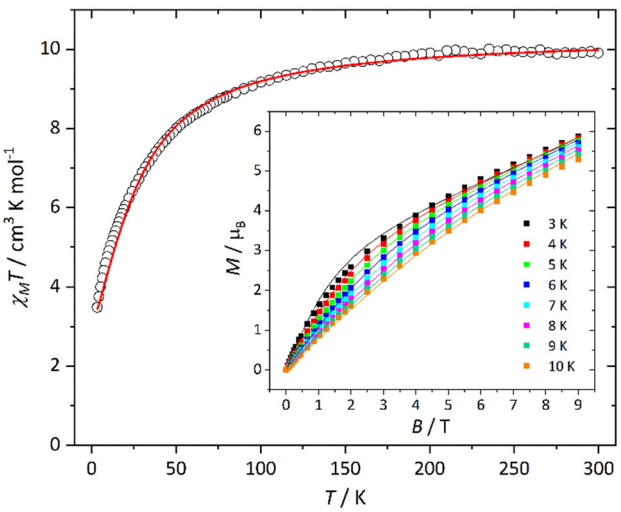

Fig. 5 Magnetic susceptibility and magnetisation (inset) data for **2**. The solid lines are a simultaneous fit of the data to spin-Hamiltonian (1). See text for full details.

At 300 K, the χT value of ~19.8 cm^3 K mol^{-1} for **2** is slightly below the value expected for four Mn^{III} ions and two Mn^{II} ions (20.75 cm^3 K mol^{-1}) with g = 2.0 (Fig. 5). Upon cooling, the χT product is essentially invariant until approximately T = 200 K wherefrom it slowly decreases to a value of ~17.4 cm^3 mol^{-1} K at T = 75 K, before decreasing more rapidly below this temperature to a value of ~6.3 cm^3 K mol^{-1} at T = 2 K. Magnetisation data rise in a near linear-like fashion without saturating; the maximum value being M = 11.7 μ_B at T = 3 K and B = 9.0 T. These data are indicative of weak antiferromagnetic exchange between neighbouring metal ions. An examination of the magnetic core of **2** reveals two 'linear' and asymmetric [Mn^{III}–Mn^{II}–Mn^{III}] trimers that are not connected to each other (Fig. S5 and S8†). Thus, we simultaneously fitted the susceptibility and magnetisation data to a model containing three metal ions and two distinct J values to spin-Hamiltonian (1) which afforded the best fit values J_1 = +0.10 cm^{-1}, J_2 = −2.52 cm^{-1}, $|D_{Mn(III)}|$ = 3.75 cm^{-1}. The larger (and negative) J_2 value reflects the larger Mn–O(Ph)–Mn (~118° *vs.* 109°) angles present. The signs/magnitudes of the exchange are in agreement with that found in calix[4]arene supported Mn clusters with similar Mn^{III}–O–Mn^{II} motifs.[10]

Conclusions

Employment of *p*-^{t}Bu-calix[4]arene (H_4TBC[4]) and 2,2′-bis-*p*-^{t}Bu-calix[4]arene (H_8-bisTBC[4]) in Mn–Na chemistry leads to the isolation of $[Mn^{III}_3Na_6(TBC[4])_3(CO_3)(Cl)(dmso)_7]\cdot 5MeCN$ ([Mn_3Na_6]; **1**·5MeCN) and $[Mn^{III}_4Mn^{II}_2Na_6(BisTBC[4])_2(CO_3)_2(Cl)_2(dmf)_8(MeOH)_{1.2}(H_2O)_{0.8}]\cdot 6MeCN$ ([Mn_6Na_6]; **2**·6MeCN), respectively. The metallic skeleton of **1** describes a tricapped trigonal prism, and that of **2** a tetracapped square prism. The change from a calix[4]arene to a bis-calix[4]arene enables expansion from three Mn^{III}-TBC[4] metalloligands in **1** to four Mn^{III}-TBC[4] metalloligands in **2**

and thus the self-assembly of a larger species. In each case the Mn^{III} ions sit in the TBC[4] polyphenolic pockets and act as capping atoms in the prism/metallic skeleton, with the Na and Na/Mn^{II} ions defining the vertices of the prism. The carbonate present in both structures results from CO_2 fixation, with yields considerably improved through deliberate addition of $Na_2CO_3/NaHCO_3$. The formation of **1** and **2** follows established binding rules in calix[4]arene coordination chemistry in which (under ambient conditions) the ligand preferentially binds Mn^{III} ions over Mn^{II} and Na^{I} ions.[9] Alongside the preferential electrostatic interaction, the tetraphenolic ligand pocket is particularly suited to accommodating four short equatorial bonds and thus the axially elongated (Jahn–Teller distorted), octahedral or square pyramidal Mn^{III} ion. The structural similarities of **1** to $[Cu^{II}_9]$ and of **2** to $[Cu^{II}_{13}]$ highlights the dominant structural role played by the calix[4]arene ligands, and their ability to form both heterometallic and heterovalent cages whilst maintaining analogous topologies. Magnetic susceptibility and magnetisation measurements reveal that **1** behaves as a paramagnet – the long distances between Mn^{III} ions connected by a single, disordered $[CO_3]^{2-}$ ion resulting in negligible magnetic exchange. Magnetic data for **2** show weak antiferromagnetic exchange in the 'linear' $[Mn^{III}–Mn^{II}–Mn^{III}]$ trimers present, with values in the range $0.10\ cm^{-1} < J < -2.52\ cm^{-1}$, consistent with previous TBC[4]-supported $Mn^{III/II}$ clusters with similar $Mn^{III}–O–Mn^{II}$ bridging angles.

Data availability

Crystallographic data for compounds **1–2** have been deposited at the CCDC under numbers 2430896 and 2430897. Further data supporting this manuscript have been included as part of the ESI.†

Author contributions

LRBW performed the synthesis, measured the PXRD data, collected and fitted magnetic data. SJD collected and solved the single crystal XRD data. EKB and SJD conceived the idea. All authors contributed to writing/editing the manuscript.

Conflicts of interest

There are no conflicts to declare.

Acknowledgements

EKB thanks the Leverhulme Trust (RPG-2021-176).

Notes and references

1 C. D. Gutsche, in *Calixarenes: An Introduction*, The Royal Society of Chemistry, Cambridge, 2nd edn, 2008, ch. 2, pp. 27–160.
2 *Calixarenes and Beyond*, ed. P. Neri, J. L. Sessler and M.-X. Wang, Springer International Publishing, Switzerland, 2016.
3 J. Vicens and J. Harrowfield, *Calixarenes in the nanoworld*, Springer, Dordrecht, Netherlands, 2006.
4 L. Mandolini and R. Ungaro, *Calixarenes in action*, Imperial College Press, London, 2000.
5 G. Sachdeva, D. Vaya, C. M. Srivastava, A. Kumar, V. Rawat, M. Singh, M. Verma, P. Rawat and G. K. Rao, *Coord. Chem. Rev.*, 2022, **472**, 214791.
6 O. Santoro and C. Redshaw, *Coord. Chem. Rev.*, 2021, **448**, 214173.
7 J. B. Simões, D. L. da Silva, S. A. Fernandes and Â. de Fátima, *Eur. J. Org. Chem.*, 2022, e202200532.
8 A. R. Kongor, V. A. Mehta, K. M. Modi, M. K. Panchal, S. A. Dey, U. S. Panchal and V. K. Jain, Calix-Based Nanoparticles: A Review, *Top. Curr. Chem.*, 2016, **374**, 28.
9 L. R. B. Wilson, M. Coletta, M. Evangelisti, S. Piligkos, S. J. Dalgarno and E. K. Brechin, *Dalton Trans.*, 2022, **51**, 4213.
10 G. Karotsis, S. J. Teat, W. Wernsdorfer, S. Piligkos, S. J. Dalgarno and E. K. Brechin, *Angew. Chem., Int. Ed.*, 2009, **48**, 8285.
11 L. R. B. Wilson, A. B. Canaj, D. J. Cutler, L. J. McCormick McPherson, S. J. Coles, H. Nojiri, M. Evangelisti, J. Schnack, S. J. Dalgarno and E. K. Brechin, *Angew. Chem., Int. Ed.*, 2024, **63**, e202405666.
12 G. Karotsis, M. Evangelisti, S. J. Dalgarno and E. K. Brechin, *Angew. Chem., Int. Ed.*, 2009, **48**, 9928.
13 M. A. Palacios, R. McLellan, C. M. Beavers, S. J. Teat, H. Weihe, S. Piligkos, S. J. Dalgarno and E. K. Brechin, *Chem. – Eur. J.*, 2015, **21**, 11212.
14 M. Coletta, S. Sanz, D. J. Cutler, S. J. Teat, K. J. Gagnon, M. K. Singh, E. K. Brechin and S. J. Dalgarno, *Dalton Trans.*, 2020, **49**, 14790.
15 S. M. Taylor, J. M. Frost, R. McLellan, R. D. McIntosh, E. K. Brechin and S. J. Dalgarno, *CrystEngComm*, 2014, **16**, 8098.
16 S. M. Taylor, R. D. McIntosh, C. M. Beavers, S. J. Teat, S. Piligkos, S. J. Dalgarno and E. K. Brechin, *Chem. Commun.*, 2011, **47**, 1440.
17 S. M. Taylor, G. Karotsis, R. D. McIntosh, S. Kennedy, S. J. Teat, C. M. Beavers, W. Wernsdorfer, S. Piligkos, S. J. Dalgarno and E. K. Brechin, *Chem. – Eur. J.*, 2011, **17**, 7521.
18 S. M. Taylor, R. D. McIntosh, S. Piligkos, S. J. Dalgarno and E. K. Brechin, *Chem. Commun.*, 2012, **48**, 11190.
19 R. McLellan, M. A. Palacios, S. Sanz, E. K. Brechin and S. J. Dalgarno, *Inorg. Chem.*, 2017, **56**, 10044.
20 M. Coletta, M. A. Palacios, E. K. Brechin and S. J. Dalgarno, *Chemistry*, 2020, **2**, 253.
21 L. T. Carroll, P. Aru Hill, C. Q. Ngo, K. P. Klatt and J. L. Fantini, *Tetrahedron*, 2013, **69**, 5002.
22 L. R. B. Wilson, M. Coletta, R. Jose, G. Rajaraman, S. J. Dalgarno and E. K. Brechin, *Dalton Trans.*, 2021, **50**, 17566.
23 M. Coletta, R. McLellan, A. Waddington, S. Sanz, K. J. Gagnon, S. J. Teat, E. K. Brechin and S. J. Dalgarno, *Chem. Commun.*, 2016, **52**, 14246.
24 R. McLellan, M. A. Palacios, C. M. Beavers, S. J. Teat, S. Piligkos, E. K. Brechin and S. J. Dalgarno, *Chem. – Eur. J.*, 2015, **21**, 2804.

25 M. Coletta, S. Sanz, L. J. McCormick, S. J. Teat, E. K. Brechin and S. J. Dalgarno, *Dalton Trans.*, 2017, **46**, 16807.
26 M. Coletta, S. Sanz, E. K. Brechin and S. J. Dalgarno, *Dalton Trans.*, 2020, **49**, 9882.
27 G. M. Sheldrick, *Acta Crystallogr., Sect. C:Struct. Chem.*, 2015, **71**, 3.
28 O. V. Dolomanov, L. J. Bourhis, R. J. Gildea, J. A. K. Howard and H. Puschmann, *J. Appl. Crystallogr.*, 2009, **42**, 339.
29 G. M. Sheldrick, *Acta Crystallogr., Sect. A*, 2015, **71**, 3.
30 G. Karotsis, S. Kennedy, S. J. Dalgarno and E. K. Brechin, *Chem. Commun.*, 2010, **46**, 3884.
31 G. D. Andreetti, R. Ungaro and A. Pochini, *J. Chem. Soc., Chem. Commun.*, 1979, 1005–1007; E. B. Brouwer, G. D. Enright and J. A. Ripmeester, *J. Am. Chem. Soc.*, 1997, **119**, 5404–5412; J. L. Atwood, L. J. Barbour, A. Jerga and B. L. Schottel, *Science*, 2002, **298**, 1000–1002.
32 A. Abragam and B. Bleaney, *Electron Paramagnetic Resonance of Transition Ions*, Clarendon Press, Oxford, 1970.